

Strongly Enhanced Vortex Pinning by Conformal Crystal Arrays

D. Ray^{1,2}, C. J. Olson Reichhardt², B. Jankó¹, and C. Reichhardt²

¹*Department of Physics, University of Notre Dame, Notre Dame, Indiana 46556*

²*Theoretical Division, Los Alamos National Laboratory, Los Alamos, New Mexico 87545*

(Dated: August 8, 2018)

Conformal crystals are non-uniform structures created by a conformal transformation of regular two-dimensional lattices. We show that gradient-driven vortices interacting with a conformal pinning array exhibit substantially stronger pinning effects over a much larger range of field than found for random or periodic pinning arrangements. The pinning enhancement is partially due to matching of the critical flux gradient with the pinning gradient, but the preservation of the sixfold ordering in the conformally transformed hexagonal lattice plays a crucial role. Our results can be generalized to a wide class of gradient-driven interacting particle systems such as colloids on optical trap arrays.

PACS numbers: 74.25.Wx, 74.25.Uv

One of the most important problems for applications of type-II superconductors is how to create high critical currents or strong vortex pinning over a wide range of applied magnetic fields¹. For over sixty years, it has been understood that the ground state vortex structure is a hexagonal lattice², so many methods have been developed to increase the critical current using uniform pinning arrays that incorporate periodicity to match the vortex structure^{3–13}. The pinning is enhanced at commensurate fields when the number of vortices equals an integer multiple of the number of pinning sites, but away from these specific matching fields, the enhancement of the critical current is lost¹⁴. Efforts to enhance the pinning at incommensurate fields have included the use of quasicrystalline substrates¹⁵ or diluted periodic arrays^{16–20}, where studies show that new types of non-integer commensurate states can arise in addition to the integer matching configurations. Hyperbolic tessellation arrays were also recently considered²¹.

Part of the problem is the fact that under an applied current, the vortex structure does not remain uniform but instead develops a Bean-like flux gradient²²: the vortex density is highest at the edges of the sample when the magnetic field is increased, and highest in the center of the sample when the magnetic field is removed and only trapped flux remains inside the sample. As a consequence, uniform pinning arrays generally have a portion of the pinning sites that are not fully occupied, suggesting that a more optimal pinning arrangement should include some type of density gradient to match the critical flux gradient. Here we show that a novel type of pinning structure, created using a conformal transformation of a uniform hexagonal lattice, produces a much higher critical current over a much wider range of magnetic fields than any pinning geometry considered up until now. Conformal crystals not only have a density gradient, but also preserve aspects of the hexagonal ordering naturally adopted by the vortex lattice. The pinning enhancement we find is substantial and will be very important for a wide range of superconductor applications and flux control. Our results can also be important for stabilizing novel self-assembled structures created using

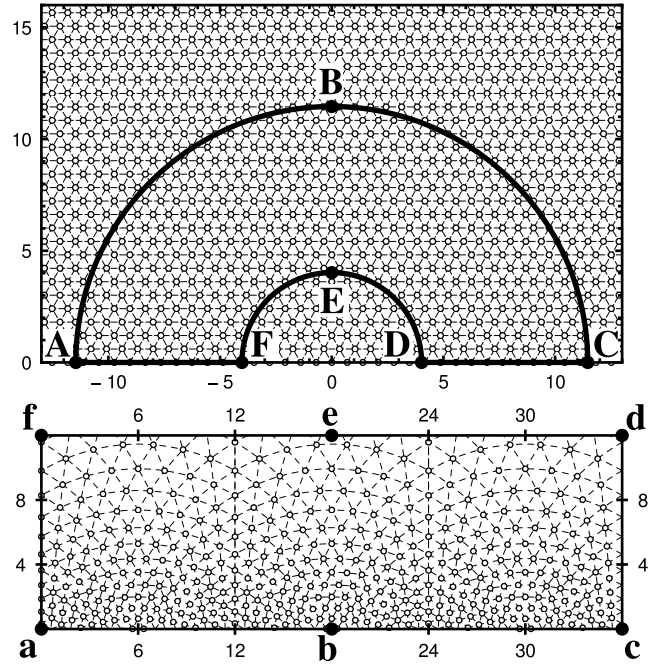


Figure 1: A conformal transformation is applied to the semi-annular section of a regular hexagonal lattice shown in (a) to create the conformal crystal structure shown in (b)²⁷. Points $A - F$ in (a) are mapped by the transformation to points $a - f$ in (b) respectively. The straight contour lines connecting nearest neighbor lattice points in (a) are bent into arcs in (b), but the local six-fold ordering of the lattice points is maintained. Pinning sites are placed at the vertices formed by the intersections of the contour lines in (b).

density gradients, such as in colloidal systems²³.

To examine vortex pinning by conformal crystalline substrates, we numerically compute the magnetization M , which is a measure of the pinning strength. We compare the effectiveness of the conformal pinning to that of random and periodic pinning arrays with the same number of pinning sites. The conformal array produces significantly stronger pinning over a much larger range of

fields than these other arrays, with the exception that the pinning by periodic arrays is strongest only in the vicinity of the matching fields¹⁴. By comparing our results to those obtained for random pinning with an equivalent gradient, we demonstrate that it is not simply the non-uniform density of the conformal array that gives rise to the pinning enhancement; rather, it is the preservation of the hexagonal ordering of the pinning by the conformal map that plays the most critical role. Another feature that gives the conformal pinning an advantage over periodic pinning for incommensurate fields is that even though local hexagonal ordering is present, the overall arc-like arrangement of the pinning sites (apparent in Figs. 1(b) and 2) prevents the formation of straight-line channels along which vortices can easily flow. In addition to vortex pinning in type-II superconductors, the effects of conformal crystalline substrates on ordering or dynamics of a monolayer of particles could also be studied for vortices in Bose-Einstein condensates on optical lattices²⁴ or colloidal particles on optically created substrate arrays²³. The enhanced pinning also suggests that conformal arrays could be used to increase friction for particle-surface interactions.

Conformal crystals are a class of two-dimensional (2D) structures created by the application of a conformal (angle-preserving) transformation to a regular lattice in the complex plane^{25,26}. Figure 1 illustrates a conformal crystal obtained via the transformation of a hexagonal lattice. The contour lines connecting nearest neighbors, which are straight lines for the original hexagonal lattice, are bent into arcs but still cross at angles of $\pi/3$, preserving the sixfold coordination of individual pinning sites in spite of the clear density gradient. To create a pinning lattice, we place pinning sites at the vertex locations where the contour lines intersect. Conformal crystal structures have been studied experimentally for repulsively interacting magnetic spheres confined to a 2D container that is tilted so that the gravitational force on the particles produces a mechanically stable but nonuniform crystal²⁶. Other systems where conformal crystals arise include foams under an external field^{28,29} and large arrays of classical Coulomb charges in confined circular potentials where local triangular ordering occurs along curved lattice lines³⁰.

Simulation— We conduct a flux gradient density simulation of the type previously used to study vortex critical states and magnetization with random^{31,32} and periodic pinning arrays¹⁴. Figure 2 shows the outer pin-free region surrounding a central pinned region that consists of two conformal crystals placed with their highest density regions adjacent to the pin-free region. Details on the construction of the conformal crystal are given in the supplemental material²⁷. We use periodic boundary conditions in the x and y -directions and consider a $36\lambda \times 36\lambda$ system with pinned region extending from $x = 6\lambda$ to 30λ , where λ is the penetration depth. This geometry was previously shown to be large enough to capture accurately the behavior of the magnetization curves^{14,31,32}.

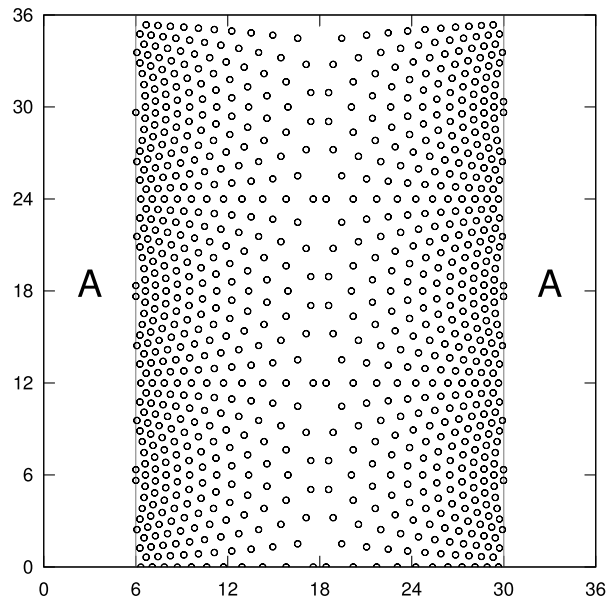


Figure 2: The gradient-driven sample geometry consists of two conformal crystals facing each other in the pinned region. Open circles are pinning site locations. Vortices are added to or subtracted from the pin-free region labeled “A” on the left and right sides of the image.

The dynamics of vortex i are obtained by integrating the overdamped equation $\eta(d\mathbf{R}_i/dt) = \mathbf{F}_i^{vv} + \mathbf{F}_i^{vp}$. η is the damping constant which is set equal to unity. The vortex-vortex interaction force is $\mathbf{F}_i^{vv} = \sum_{j=1}^{N_v} s_i s_j F_0 K_1(R_{ij}/\lambda) \hat{\mathbf{R}}_{ij}$, where K_1 is the modified Bessel function, \mathbf{R}_i is the location of vortex i , $R_{ij} = |\mathbf{R}_i - \mathbf{R}_j|$, $\hat{\mathbf{R}}_{ij} = (\mathbf{R}_i - \mathbf{R}_j)/R_{ij}$, $F_0 = \phi_0^2 \pi \mu_0 \lambda^3$, and ϕ_0 is the elementary flux quantum. The sign prefactor s_i is $+1$ for a vortex and -1 for an antivortex. The pinning sites are modeled as N_p non-overlapping parabolic traps with $\mathbf{F}_i^{vp} = \sum_{k=1}^{N_p} (F_p R_{ik}^p / R_p) \Theta((R_p - R_{ik}^p)/\lambda) \hat{\mathbf{R}}_{ik}^p$, where R_{ik}^p is the location of pinning site k , $R_{ik}^p = |\mathbf{R}_i - \mathbf{R}_k^p|$, $\hat{\mathbf{R}}_{ik}^p = (\mathbf{R}_i - \mathbf{R}_k^p)/R_{ik}^p$, Θ is the Heaviside step function, R_p is the pinning radius that we fix to $R_p = 0.12\lambda$, and F_p is an adjustable parameter controlling the strength of the pinning force. All forces are measured in units of F_0 and all lengths in units of λ . The external field is measured in units of H_ϕ , the field at which the average unit density of vortices equals the average unit density of pinning sites.

To perform a complete field sweep, we begin with zero vortex density and then quasistatically add vortices in the unpinned region (labeled “A” in Fig. 2) at randomly chosen nonoverlapping positions until the desired maximum external field value is reached. As the vortex or antivortex density builds up in the pin-free region, the vortices or antivortices drive themselves into the pinned region due to their own repulsive interactions, creating a gradient in the flux density within the pinned region^{14,31,32}. We then remove vortices from the pin-free region until the vortex density in this region reaches

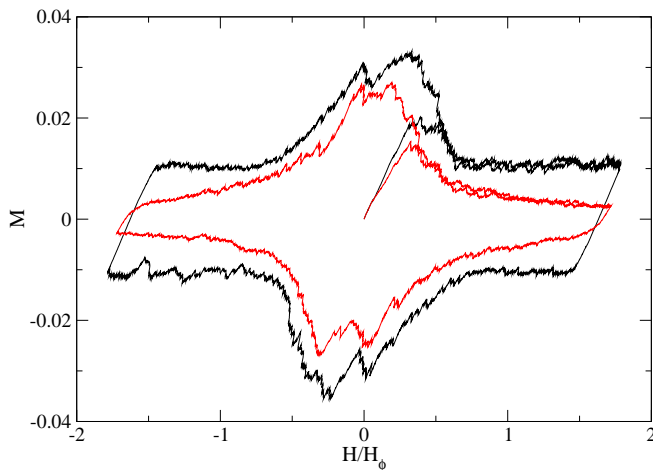


Figure 3: The magnetization M vs H/H_ϕ , where H_ϕ is the matching field at which the vortex density equals the average pinning density, in samples with $n_p = 1.0$ and $F_p = 0.55$. Outer dark (black) curve: a sample with a conformal pinning array (CPA). Inner light (red) curve: a sample with a uniformly dense random arrangement of pinning sites. The CPA produces a much higher value of M at all fields.

zero. To reverse the field, we add antivortices, which repel each other but are attracted to vortices, to the unpinned region. When a vortex and antivortex come within a small distance (0.3λ) of each other, they are both removed from the system to simulate an annihilation event. To complete an entire magnetization loop, we continue to add anti-vortices until the external field reaches its most negative value, and then remove antivortices from the pin-free region to bring the external field back up to zero. The average magnetization M is calculated as the difference between the flux density H in the unpinned region and the density B in the pinned region, $M = -(1/4\pi V) \int (H - B) dV$, where V is the sample area. The critical current J_c is proportional to the magnetization.

Results— In Fig. 3 we plot the complete hysteresis loop M vs H/H_ϕ for the conformal pinning array (CPA) and the uniformly dense random pinning array. Each sample contains the same number N_p of pinning sites with an average pinning density of $n_p = 1.0$ and with $F_p = 0.55$. We find that M is much higher at all fields for the CPA than for the random pinning, and that at its highest point, M for the CPA is almost four times higher than for the random pinning. Although the CPA has local triangular ordering, we observe no peaks or other anomalies in M at integer matching or fractional matching multiples of H/H_ϕ of the type found for uniformly dense periodic pinning arrays¹⁴. The flux profiles plotted in Suppl. Fig. 1²⁷ show that the random array produces a Bean-like profile that becomes shallower as H increases. In contrast, at higher fields the CPA does not have a uniform flux gradient but instead develops a double slope profile, with a larger flux gradient near the edge of the sample and

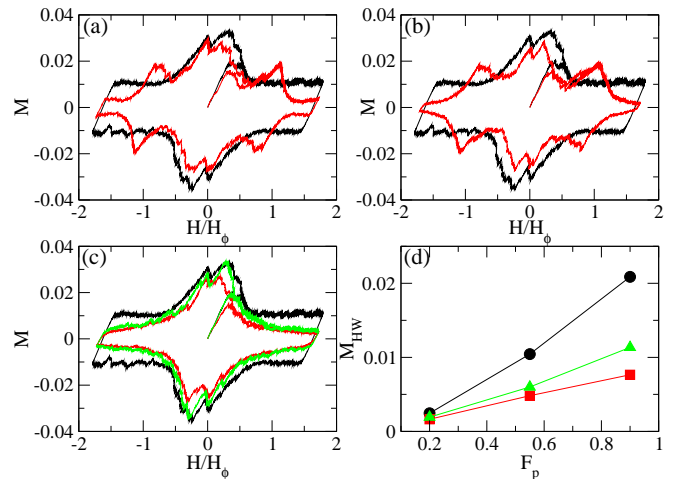


Figure 4: (a-c) M vs H/H_ϕ plots for samples with $F_p = 0.55$ and average pin density $n_p = 1.0$. (a) Dark (black) curve: the CPA system from Fig. 3; light (red) curve: a uniform square pinning array. (b) Dark (black) curve: the CPA system; light (red) curve: a uniform triangular pinning array. M is higher for both the uniform periodic pinning systems than for the CPA at the matching field near $H/H_\phi = 1.0$, but the CPA has the highest value of M at all other fields. (c) Outer dark (black) curve: the CPA system; middle light (green) curve: a random arrangement of pinning sites with an equivalent pinning gradient; inner light (red) curve: the uniform random array. Here the gradient in the random pinning increases M compared to the uniform random pinning by only a small amount for most fields. (d) M_{HW} , the half-width of the magnetization loop at $H/H_\phi = 1.0$, for the CPA (circles), random array with CPA-equivalent pinning gradient (triangles), and uniform random pinning array (squares) for varied F_p . There is a consistent enhancement of M in the CPA.

a much shallower or nearly flat flux profile in the center of the sample. As H increases, the sharper slope region decreases in width and is replaced by the shallow slope region. We have examined a range of pinning forces and find that the magnetization for the CPA is consistently higher than for random pinning arrays, as shown in Fig. 4(d) where we plot M_{HW} , the half-width of the magnetization loop at $H/H_\phi = 1.0$, at varied F_p for these array types.

We next address whether the conformal pinning arrays produce higher pinning compared to other previously studied types of non-random pinning arrays. In Fig. 4(a) we plot M vs H/H_ϕ for the CPA and a square pinning array with the same pinning density and strength, and in Fig. 4(b) we plot the same quantity for the CPA and a triangular pinning array. In both cases, M for the CPA is higher over most of the range of H/H_ϕ except at the first matching field, where the periodic pinning arrays produce a higher value of M due to a commensurability effect. This shows that although a periodic pin structure can strongly enhance the pinning, this enhancement occurs only for a very specific matching field. In contrast, the CPA produces a significant enhancement of the pin-

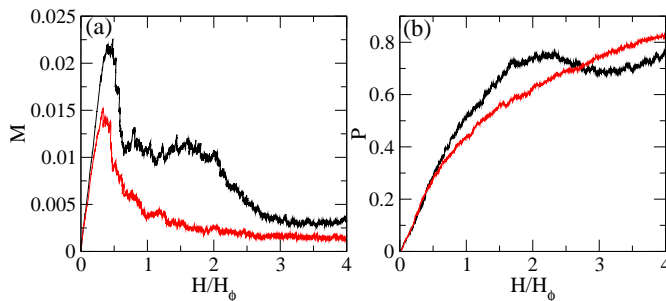


Figure 5: (a) The high field behavior of M vs H/H_ϕ for samples with $F_p = 0.55$ and $n_p = 1.0$ on the initial ramp up only. Dark (black) curve: CPA; light (red) curve: uniform random array. Although M is higher for the CPA than for the random array over the entire range of fields, there is a drop in M for $H/H_\phi > 2.0$ in the CPA. (b) The fraction of occupied pinning sites P vs H/H_ϕ for the CPA (dark black curve) and uniform random pinning (light red curve). P is initially higher for the CPA but drops at $H/H_\phi = 2$, coinciding with the drop in M in (a), while P for the random pinning sample increases monotonically with increasing field.

ning over a very broad range of fields, extending well above the first matching field.

Since the CPA has a pinning gradient, it could be possible that any type of pinning array with an equivalent gradient would also exhibit a pinning enhancement compared to uniform pinning arrays and could be just as efficient at pinning as the CPA. We find that this is not the case. In Fig. 4(c) we plot M versus H/H_ϕ for the CPA and a random pinning array with an equivalent pinning gradient and the same average pinning density. For comparison we also show the uniform random pinning array. The random pinning with a gradient exhibits a modest enhancement of M compared to the uniform random pinning array; however, both arrays give M values that are significantly smaller than the CPA for all but the very lowest fields. This result indicates that it is the other properties of the CPA such as the preservation of local sixfold ordering, and not merely the pinning gradient, that are responsible for the enhanced pinning. The arching structure of the CPA suppresses certain modes of vortex motion. For example, for random pinning arrays it has been found that certain regions where the pinning density is slightly lower lead to the formation of persistent river-like flow patterns³²; these structures are unable to form in the CPA. For periodic pinning arrangements, easy vortex flow occurs along the symmetry directions of the pinning array^{33,34}, causing a drop in the critical current above a commensurate field. Such motion is suppressed in the CPA due to the arching structure.

In Fig. 5(a) we compare M versus H/H_ϕ for the CPA and uniform random arrays in the first quarter of the magnetization loop over a much larger range of fields up to $H/H_\phi = 4.0$, and in Fig. 5(b) we plot the correspond-

ing pin occupancy P , which is the fraction of pinning sites occupied by vortices. The enhanced pinning for the CPA is the most pronounced below $H/H_\phi = 2.0$. The enhancement decreases above this field but remains larger than the random pinning array for all fields. For the random pinning array, P monotonically increases over the entire range of H/H_ϕ . In contrast, after running well above the P value for the random pinning array at lower fields, P for the CPA rolls over and begins to decrease with increasing field above $H/H_\phi \approx 2$, correlated with the decrease in M . This is also the field at which the higher gradient region seen in Suppl. Fig. 1(a) disappears from the sample²⁷. Just below this field, all of the pinning sites near the edge of the sample are occupied, and since these pinning sites are the most closely spaced, as additional vortices enter the sample, the vortex-vortex interactions become strong enough to push some of the vortices out of the pins, leading to the drop in P and M . For the random pinning array, there are always some empty pinning sites near the edge of the sample in places where two pins happen to be in close proximity, so that the vortex-vortex interaction energy would be prohibitively high if both pins were occupied simultaneously. As the field increases, these pinning sites gradually become occupied. Even though P for the CPA falls below P for the random array at higher fields, the pinning enhancement remains significantly stronger for the CPA.

In summary, we demonstrate strongly enhanced vortex pinning by a conformal crystal array of pinning sites. The conformal crystal is constructed by a conformal transformation of a hexagonal lattice, producing a nonuniform structure with a gradient where the local sixfold coordination of the pinning sites is preserved, and with an arching effect. The conformal pinning arrays produce significantly enhanced pinning over a much wider range of field than that found for other pinning geometries with an equivalent number of pinning sites, such as random, square, and triangular. We show that the pinning enhancement is not simply due to the pin density gradient, but is also due to the preservation of the sixfold coordination of the pinning sites and to the arching effects that prevent the formation of easy channels of vortex flow. The conformal pinning arrays do not show any pronounced enhancement at the matching fields of the type found for periodic pinning arrays; however, there is a drop in the magnetization at higher fields that is correlated with a drop in the occupancy of the pinning sites. Our results will be important for applications where high critical currents are required, and can be generalized to stabilizing or pinning other systems, such as colloidal particles, that do not form uniform crystalline structures.

This work was carried out under the auspices of the NNSA of the U.S. DoE at LANL under Contract No. DE-AC52-06NA25396.

-
- ¹ G. Blatter, M.V. Feigel'man, V.B. Geshkenbein, A.I. Larkin, and V.M. Vinokur, *Rev. Mod. Phys.* **66**, 1125 (1994).
- ² A.A. Abrikosov, *Rev. Mod. Phys.* **76**, 975 (2004).
- ³ M. Baert, V.V. Metlushko, R. Jonckheere, V.V. Moshchalkov, and Y. Bruynseraede, *Phys. Rev. Lett.* **74**, 3269 (1995).
- ⁴ V. Metlushko, U. Welp, G.W. Crabtree, R. Osgood, S.D. Bader, L.E. DeLong, Z. Zhang, S.R.J. Brueck, B. Ilic, K. Chung, and P. J. Hesketh, *Phys. Rev. B* **60**, R12585 (1999).
- ⁵ S.B. Field, S.S. James, J. Barentine, V. Metlushko, G. Crabtree, H. Shtrikman, B. Ilic, and S.R.J. Brueck, *Phys. Rev. Lett.* **88**, 067003 (2002); A.N. Grigorenko, S.J. Bending, M.J. Van Bael, M. Lange, V.V. Moshchalkov, H. Fangohr, and P.A.J. de Groot, *ibid.* **90**, 237001 (2003).
- ⁶ U. Welp, Z.L. Xiao, J.S. Jiang, V.K. Vlasko-Vlasov, S.D. Bader, G.W. Crabtree, J. Liang, H. Chik, and J.M. Xu, *Phys. Rev. B* **66**, 212507 (2002); U. Welp, Z.L. Xiao, V. Novosad, and V.K. Vlasko-Vlasov, *Phys. Rev. B* **71**, 014505 (2005).
- ⁷ G. Karapetrov, J. Fedor, M. Iavarone, D. Rosenmann, and W.K. Kwok, *Phys. Rev. Lett.* **95**, 167002 (2005).
- ⁸ J.I. Martín, M. Vélez, A. Hoffmann, I.K. Schuller, and J.L. Vicent, *Phys. Rev. Lett.* **83**, 1022 (1999); W.J. Zhang *et al.*, *EPL* **99**, 37006 (2012).
- ⁹ J.I. Martín, M. Vélez, J. Nogués, and I.K. Schuller, *Phys. Rev. Lett.* **79**, 1929 (1997); D.J. Morgan and J.B. Ketterson, *ibid.* **80**, 3614 (1998); J.E. Villegas, E.M. Gonzalez, Z. Sefrioui, J. Santamaria, and J. L. Vicent, *Phys. Rev. B* **72**, 174512 (2005).
- ¹⁰ K. Harada, O. Kamimura, H. Kasai, T. Matsuda, A. Tonomura, and V.V. Moshchalkov, *Science* **274**, 1167 (1996); C. Reichhardt, C.J. Olson, and F. Nori, *Phys. Rev. B* **57**, 7937 (1998); G.R. Berdiyrov, M.V. Milosevic, and F.M. Peeters, *Phys. Rev. Lett.* **96**, 207001 (2006).
- ¹¹ S. Goldberg *et al.*, *Phys. Rev. B* **79**, 064523 (2009); G. Shaw, B. Bag, S.S. Banerjee, H. Suderow, and T. Tamegai, *Supercond. Sci. Technol.* **25**, 095016 (2012).
- ¹² J.I. Vestgarden, V.V. Yurchenko, R. Wördenweber, and T.H. Johansen, *Phys. Rev. B* **85**, 014516 (2012).
- ¹³ I. Swiecicki, C. Ulysse, T. Wolf, R. Bernard, N. Bergeal, J. Briatico, G. Faini, J. Lesueur, and J.E. Villegas, *Phys. Rev. B* **85**, 224502 (2012).
- ¹⁴ C. Reichhardt, J. Groth, C.J. Olson, S.B. Field, and F. Nori, *Phys. Rev. B* **54**, 16108 (1996).
- ¹⁵ V. Misko, S. Savel'ev, and F. Nori, *Phys. Rev. Lett.* **95**, 177007 (2005); M. Kemmler, C. Gürlich, A. Sterck, H. Pöhler, M. Neuhaus, M. Siegel, R. Kleiner, and D. Koelle, *Phys. Rev. Lett.* **97**, 147003 (2006); A.V. Silhanek, W. Gillijns, V.V. Moshchalkov, B.Y. Zhu, J. Moonens, and L.H.A. Leunissen, *Appl. Phys. Lett.* **89**, 152507 (2006); J.E. Villegas, M.I. Montero, C.-P. Li, and I.K. Schuller, *Phys. Rev. Lett.* **97**, 027002 (2006); C. Reichhardt and C. J. Olson Reichhardt, *Phys. Rev. Lett.* **106**, 060603 (2011).
- ¹⁶ C. Reichhardt and C. J. Olson Reichhardt, *Phys. Rev. B* **76**, 094512 (2007).
- ¹⁷ M. Kemmler, D. Bothner, K. Ilin, M. Siegel, R. Kleiner, and D. Koelle, *Phys. Rev. B* **79**, 184509 (2009).
- ¹⁸ Y.J. Rosen, A. Sharoni, and I.K. Schuller, *Phys. Rev. B* **82**, 014509 (2010).
- ¹⁹ C. Reichhardt and C.J. Olson Reichhardt, *Phys. Rev. B* **76**, 064523 (2007).
- ²⁰ A.D. Thakur, S. Ooi, S.P. Chockalingam, J. Jesudasan, P. Raychaudhuri, and K. Hirata, *Appl. Phys. Lett.* **94**, 262501 (2009).
- ²¹ V.R. Misko and F. Nori, *Phys. Rev. B* **85**, 184506 (2012).
- ²² C.P. Bean, *Rev. Mod. Phys.* **36**, 32 (1964).
- ²³ P.T. Korda, G.C. Spalding, and D.G. Grier, *Phys. Rev. B* **66**, 024504 (2002); K. Mangold, P. Leiderer, and C. Bechinger, *Phys. Rev. Lett.* **90**, 158302 (2003).
- ²⁴ S. Tung, V. Schweikhard, and E.A. Cornell, *Phys. Rev. Lett.* **97**, 240402 (2006).
- ²⁵ F. Rothen, P. Pieranski, N. Rivier, and A. Joyet, *Eur. J. Phys.* **14**, 227 (1993).
- ²⁶ F. Rothen and P. Pieranski, *Phys. Rev. E* **53**, 2828 (1996).
- ²⁷ See supplemental material in EPAPS Document x.
- ²⁸ W. Drenckhan, D. Weaire, and S.J. Cox, *Eur. J. Phys.* **25**, 429 (2004).
- ²⁹ M. Mancini and C. Oguey, *Eur. Phys. J. E* **17**, 119 (2005).
- ³⁰ A. Mughal and M. A. Moore, *Phys. Rev. E* **76**, 011606 (2007).
- ³¹ C. Reichhardt, C.J. Olson, J. Groth, S. Field, and F. Nori, *Phys. Rev. B* **52**, 10441 (1995).
- ³² C. Reichhardt, J. Groth, C.J. Olson, S.B. Field, and F. Nori, *Phys. Rev. B* **53**, R8898 (1996).
- ³³ A.V. Silhanek, J. Gutierrez, R.B.G. Kramer, G.W. Ataklti, J. Van de Vondel, V.V. Moshchalkov, and A. Sanchez, *Phys. Rev. B* **83**, 024509 (2011).
- ³⁴ C. Reichhardt and C.J. Olson Reichhardt, *Phys. Rev. B* **79**, 134501 (2009).

SUPPLEMENTARY MATERIAL

for “Strongly Enhanced Vortex Pinning by
Conformal Crystal Arrays”

**I. CONSTRUCTION OF THE CONFORMAL
CRYSTAL**

To obtain the conformal crystal structure, we first situate a regular hexagonal lattice in the complex plane: that is, we encode the location (x, y) of each lattice site into a complex number $z = x + iy$. With lattice constant b , the lattice sites will be located at

$$z = n_1 \cdot (1 \cdot b) + n_2 \cdot \left(e^{i\pi/3} \cdot b \right) \quad (1)$$

where n_1 and n_2 are arbitrary integers.

We then consider a semiannular region of this lattice as shown in Fig. 1(a) of the main text, defined by $\text{Im}z \geq 0$ and $r_{\text{in}} \leq |z| \leq r_{\text{out}}$, and apply a conformal (angle-preserving) transformation mapping z to $w \equiv u + iv$, given by

$$w = \frac{\pi}{2\alpha} + \frac{1}{i\alpha} \ln(iz) \quad (2)$$

where $\alpha \equiv \frac{1}{r_{\text{out}}}$. The semiannular region in the z -plane shown in Fig. 1(a) of the main text will be mapped to the rectangular region in the w -plane shown in Fig. 1(b)

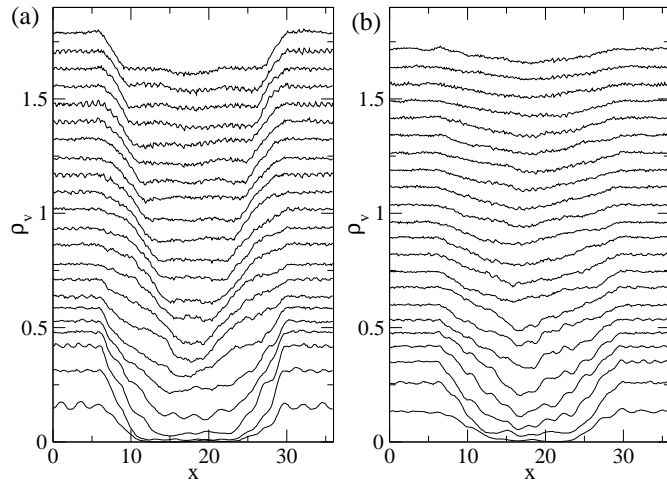


Figure 1: Data from the samples in Fig. 3 of the main text with $n_p = 1.0$ and $F_p = 0.55$. (a) The average flux density ρ_v across the sample plotted for different times during the ramp up portion of the hysteresis curve for the conformal pinning array (CPA). (b) ρ_v for the random pinning array. The random array exhibits a Bean profile while the CPA has two regions inside the sample: a higher flux gradient at the edges of the pinned region and a small gradient in the middle.

of the main text, specified by

$$0 \leq u \leq \pi r_{\text{out}} \quad \text{and} \quad 0 \leq v \leq r_{\text{out}} \ln \left(\frac{r_{\text{out}}}{r_{\text{in}}} \right).$$

A. Explicit Construction

The structure of the final conformal crystal is completely determined by specifying the three constants b , r_{out} , and r_{in} . The locations of the sites of the conformal crystal can be generated directly by the expressions

$$u = r_{\text{out}} \cdot \left\{ \frac{\pi}{2} - \tan^{-1} \left(\frac{2n_1 + n_2}{n_2\sqrt{3}} \right) \right\} \quad (3a)$$

$$v = r_{\text{out}} \ln \frac{r_{\text{out}}}{b\sqrt{n_1^2 + n_2^2 + n_1n_2}} \quad (3b)$$

where (n_1, n_2) range over all pairs of integers satisfying the two constraints, $n_2 \geq 0$ and

$$r_{\text{in}}^2 \leq b^2 (n_1^2 + n_2^2 + n_1n_2) \leq r_{\text{out}}^2.$$

To obtain a conformal crystal of length u_{max} and width v_{max} , one chooses r_{out} and r_{in} to have the values

$$r_{\text{out}} = \frac{u_{\text{max}}}{\pi}, \quad r_{\text{in}} = \frac{u_{\text{max}}}{\pi} \exp \left(-\frac{\pi v_{\text{max}}}{u_{\text{max}}} \right).$$

b can be chosen to obtain a desired final density ρ of lattice sites:

$$b^2 = \frac{1 - (r_{\text{in}}/r_{\text{out}})^2}{\rho\sqrt{3} \cdot \ln(r_{\text{out}}/r_{\text{in}})}$$

Alternatively, it can be set equal to a desired minimum distance between pinning sites in the final structure. (Note that in Fig. 1 of the main text, the lengths of arc ABC and line abc are equal.)

Figure 1 of the main text was obtained using $r_{\text{out}} = 36/\pi$, $r_{\text{in}} = r_{\text{out}}e^{-\pi/3}$, and $b^2 = (1 - \exp(-2\pi/3)) \cdot (\sqrt{3}/\pi)$. These parameter values were calculated from $u_{\text{max}} = 36$, $v_{\text{max}} = 12$, and $\rho = 1$.

II. FLUX DENSITY PROFILES

In Supplemental Fig. 1(a) we plot the flux density profiles obtained by averaging the flux density in the y direction for the first ramp up of the field in the hysteresis loop for the conformal pinning array (CPA) illustrated in Fig. 3 of the main text, and in Supplemental Fig. 1(b) we show the flux density profiles for the uniform random pinning array from Fig. 3 of the main text. The random array produces a Bean-like profile that becomes shallower as H increases. In contrast, at higher fields the CPA does not have a uniform flux gradient but instead develops a double slope profile, with a larger flux gradient near the edge of the sample and a much shallower or nearly flat flux profile in the center of the sample. As H increases, the sharper slope region decreases in width and is replaced by the shallow slope region.